Journal of Environmental Chemical Engineering 10 (2022) 107402

Contents lists available at ScienceDirect

Journal of Environmental Chemical Engineering

journal homepage: www.elsevier.com/locate/jece

# Aqueous-phase reforming of glycerol over Pt-Co catalyst: Effect of process variables

A.J. Reynoso [a], J.L. Ayastuy [a,*], U. Iriarte-Velasco [b], M.A. Gutiérrez-Ortiz [a]

[a] Department of Chemical Engineering, Faculty of Science and Technology, University of the Basque Country UPV/EHU, Sarriena S/N, 48940 Leioa, Spain
[b] Department of Chemical Engineering, Faculty of Pharmacy, University of the Basque Country UPV/EHU, Paseo de la Universidad, 7, 01006 Vitoria, Spain

ARTICLE INFO

Editor: Dr. Zhang Xiwang

*Keywords:*
Aqueous-phase reforming
Glycerol
Cobalt catalyst
Platinum
Hydrogen

ABSTRACT

This study examined the influence of process variables (glycerol concentration in feed, coupled temperature/pressure and space velocity) in the catalytic performance in the APR of glycerol over 0.3Pt/CoAl catalyst in a continuous fixed-bed reactor in order to maximize the production of $H_2$. The effect of glycerol concentration in the feed was studied from 5 to 20 wt%, the coupled temperature/pressure varied from 225 °C/25 bar to 260 °C/50 bar and the spatial velocity was changed from 0.68 to 17 $h^{-1}$. Our results reflected that $H_2$ production was favored at higher reaction temperature/pressure (3.62 vs. 2.49 $mol_{H2}/mol_{Gly\text{-}converted}$, at the most severe and mild conditions, respectively), lower WHSV (3.89 vs. 1.27 $mol_{H2}/mol_{Gly\text{-}converted}$, at the lowest and highest space velocity, respectively) and more diluted feedstocks (3.95 vs. 1.44 $mol_{H2}/mol_{Gly\text{-}converted}$, at the most diluted and concentrated freestreams, respectively). A threshold value at 10 wt% glycerol was found for the ratio of dehydrogenation to dehydration liquid products. The post-reaction catalyst was also characterized by several techniques, showing that Co leaching was the major drawback, especially at the mildest operation conditions, while carbonaceous deposits are negligible.

## 1. Introduction

The fossil-based energy system and the dependence on fossil fuels have exacerbated climate change, resulting in an environmental crisis [1]. A change in the fuel production and consumption strategies become necessary in order to reduce the greenhouse gases and other emissions responsible for the global warming. Any alternative to reduce the dependence on petroleum should address the production of energy and chemicals from renewable feedstocks, such as biomass [2]. Biomass has the potential to decrease net emissions of carbon since the used raw materials grow removing carbon dioxide from the atmosphere by photosynthesis [3].

Hydrogen production from biomass, in addition to reducing greenhouse gas emissions, would contribute to the expansion and economic viability of the biorefinery [3]. Hydrogen has been globally accepted as an environmentally friendly fuel, since huge energy is contained in the H-H bond and its combustion only releases water to the environment [4]. Moreover, hydrogen can be used in several technologies such as fuel cells and internal combustion engines or turbines [5,6]. Hydrogen can be produced effectively from biomass through a sort of processes [7–10], among which is the aqueous-phase reforming [11].

Aqueous-phase reforming (APR), which can be driven at relatively mild conditions, is able to manage diluted aqueous wastes of different oxygenated hydrocarbons to obtain valuable products (either hydrogen or other value-added chemicals) [12]. APR process was first introduced in 2002 by Dumesic and co-workers [13], and since then, had attracted a considerable R&D activities. In APR, reactants remain in liquid phase, unlike steam reforming (SR), what avoids an energetically demanding vaporization-step. Furthermore, low reaction temperatures shift the Water-Gas Shift (WGS) equilibrium towards further formation of hydrogen with the consequent reduction of carbon monoxide content [14].

Glycerol, a major by-product of the biodiesel production process, is one of the 12 platform molecules for biorefineries proposed by the US Department of Energy [15]. A huge surplus of glycerol has been generated in the last years, thus, its valorisation represents a challenge for the biodiesel plants profitability [16]. Aqueous-phase reforming of glycerol comprises the decomposition (Eq. 1) and the Water-Gas Shift (WGS) (Eq. 2) steps:

$$C_3H_8O_3 \rightarrow 4H_2 + 3CO \quad (1)$$

* Corresponding author.
*E-mail address:* joseluis.ayastuy@ehu.eus (J.L. Ayastuy).

https://doi.org/10.1016/j.jece.2022.107402
Received 24 November 2021; Received in revised form 20 January 2022; Accepted 12 February 2022
Available online 16 February 2022

$$CO + H_2O \leftrightarrow H_2 + CO_2 \quad (2)$$

The overall reaction stoichiometry for the ideal APR of glycerol is given by reaction 3:

$$C_3H_8O_3 + 3H_2O \rightarrow 7H_2 + 3CO_2 \quad (3)$$

As an immature technology, this process requires constant investigation for active and stable catalytic materials and optimization of operating conditions to improve current results to the point of being profitable for the industry [17].

Numerous works have focused on noble metal based catalysts for APR, especially Pt and Re, due to their high efficiency for C–C, O–H and C–H bonds cleavage and WGS reaction [17–24]. Thanks to its higher availability and economy, Ni-based systems have also been widely studied as an alternative to those upscale metals [25–29]. Cobalt is another transition metal that has attracted attention for this type of process [30–32]. Nevertheless, leaching is a large drawback for transition metals. Both catalytic systems, based on precious and transition metals, present a certain deactivation, mainly due to hydrothermal instabilities [33]. Among the strategies considered, bimetallic catalysts upgrade glycerol conversion and gaseous products and improve stability [30,34–37]. For instance, bimetallic Pt-Co supported on multi-walled carbon nanotubes increases the glycerol reforming activity of the monometallic catalyst by 4, and the WGS activity by 32 [30].

APR process is clearly impacted by operating variables as a substrate concentration, temperature and system pressure, and contact time, among others [38,39]. Several authors have optimized temperature and pressure conditions to enhance gaseous products [19,40–43], a few others have conducted research that address other parameters such as feed concentration, mass of catalyst/ reagent mass flow rate ratio, reaction time and feed flow rate [38,39,44]. The reported results, however, become contradictory since they depend on the interrelation with other variables and the reaction system [39]. Moreover, most of the literature is focused on catalyst performance with respect to either gas o liquid phase product distribution.

The present work aims to investigate the effect that operating conditions exert on the product distribution during the APR of glycerol over a 0.3PtCoAl catalyst, in order to maximize the hydrogen production by APR. This catalyst, synthesized by impregnating Pt on cobalt aluminate support, has been previously tested in long-term reactions (100 h TOS), proving to be efficient for $H_2$ production and stable [45]. Due to its promising performance, in this work this optimized catalyst formulation was used as a benchmark to search the suitable reaction conditions for hydrogen production. For this purpose, the most handled process variables, such as glycerol concentration in the feedstream, coupled temperature/pressure and contact time, were investigated. The catalytic performance was evaluated based on the most commonly applied reaction indices, and a comprehensive analysis of both gaseous and liquid products is presented. In addition, exhausted catalyst was also characterized to gain knowledge in the main deactivation causes.

## 2. Experimental section

### 2.1. Catalyst synthesis

Bimetallic 0.3Pt/CoAl catalyst was synthetized in two steps. First, cobalt aluminate with a nominal Co/Al mole ratio of 0.625, was synthesized by coprecipitation. An aqueous solution containing appropriate amounts of Co and Al precursors (10.3 g of $Co(NO_3)_2{\cdot}6H_2O$ and 21.2 g of $Al(NO_3)_3{\cdot}9H_2O$) was added dropwise to a vigorously stirred solution containing sodium carbonate while pH was adjusted to 10 with NaOH solution (2 M). The resulting slurry was aged for 24 h at room temperature, filtered, washed several times with de-ionized water and dried in an oven at 110 °C overnight. The cobalt aluminate spinel was formed by calcination at 500 °C (heating rate 5 °C/min) for 5 h in a static air atmosphere. Thereafter, Pt was impregnated (nominal loading 0.3 wt%) using aqueous solution of tetraammineplatinum(II) nitrate as precursor, in the solution/support proportion of 1.5/1 (vol./vol.). After impregnation, the sodden solid was dried in an oven at 110 °C for 17 h and finally, calcined at 350 °C (heating rate 5 °C/min) for 5 h.

### 2.2. Characterization of the catalyst

The bulk composition of the catalyst was evaluated by ICP-AES. The specific surface area and the main pore size were estimated by the BET and BJH methods, respectively. The measurement was performed using nitrogen at 77 K as an adsorbent gas (Tristar II 3020). Prior to the physisorption measurement, the sample was outgassed at 300 °C for 10 h in order to clean the solid surface.

XRD diffraction patterns of the calcined, reduced and spent catalyst were obtained on a PANalytical X'pert PRO diffractometer ($Cu_{K\alpha}$ radiation, $\lambda = 1.5406$ Å, graphite monochromator)), with a step size of 0.026° (2θ) and a counting time of 2 s. The crystallite average size was calculated by Scherrer equation from the peak broadening and the identification of the crystal phases was carried out on the basis of ICDD database.

$^{27}Al$ Solid State NMR measurements at 104.26 MHz for $^{27}Al$ were performed (9.4 T Bruker AVANCE III 400 spectrometer). Chemical shifts were referenced externally to the $AlCl_3$ aqueous solution at 0 ppm. The spectra were acquired at a spinning frequency of 60 kHz employing a PH MASDVT400W BL 1.3 mm ultrafast probe head.

The XPS analyses were performed on a SPECS spectrometer with Phoibos 150 1DDLD analyzer and a monochromatic X-ray beam Al K target (1486.7 eV). The electron energy analyzer was operated at pass energy of 30 eV and step size of 0.08 eV. The C 1 s photoelectron line (BE = 284.8 eV) was used to calibrate the binding energies of the photoelectron. The catalyst was analyzed either in calcined and reduced form. The reduction of the catalyst was carried out in-situ at 600 °C with 20% $H_2$/Ar flow, for 1 h.

Temperature programmed reduction of the fresh calcined ($H_2$-TPR) catalysts was carried out in a Micromeritics AutoChem 2920 apparatus, equipped with a thermal conductivity detector (TCD). About 50 mg of sample was initially heated in He stream at 550 °C for 1 h (heating rate 10 °C/min). Then, sample was cooled down to room temperature into Ar flow, and switched to 5% $H_2$/Ar flow while temperature was ramped to 950 °C at 10 °C/min, and hold for 1 h.

Temperature programmed hydrogenation (TPH) was conducted on the spent catalyst is order to analyse carbonaceous deposits. Sample was first heated at 550 °C for 1 h, under a He flow, and cooled down to ambient temperature. Then, a flow of 5% $H_2$/Ar was passed through the sample heated at 10 °C/min up to 950 °C and $m/z = 15$ ($CH_4$) signal was recorded with mass spectrometer (Pffeifer Vacuum OmniStar).

The amount of surface Pt and Co sites were evaluated by $H_2$ pulse chemisorptions (5% $H_2$/Ar, loop volume 0.5312 mL) at 40 °C (Micromeritics AutoChem 2920 equipment). Initially, catalyst surface was cleaned by passing a He flow at 500 °C. First, $H_2$ pulse was applied on sample reduced at 250 °C (to titrate the metallic Pt). Thereafter, sample was further reduced at 600 °C, and subsequent pulse chemisorption was completed (to titrate the total metallic sites). H/Me (Me=Pt, Co) stoichiometry of 1/1 was assumed. The exposed metallic area of Pt and Co ($S_{Pt}^o$ and $S_{Co}^o$) was calculated assuming 0.084 $nm^2$ and 0.0662 $nm^2$ per Pt and Co sites, respectively. The average Pt size was calculated by formula $d_{Pt}^o$ (nm) = $6000/(\rho{\cdot}S_{Pt}^o)$ [46].

The surface acid and base properties of the reduced solid were evaluated by temperature programmed desorption (TPD) of $NH_3$ and $CO_2$, respectively, conducted in a Micromeritics AutoChem 2920 equipment coupled to Mass Spectrometer (MKS Cirrus). Previously, sample was cleaned by passing a He flow at 550 °C for 1 h and cooled down to room temperature. Then, the solid was reduced at 600 °C in 5% $H_2$/Ar flow (heating rate 10 °C/min), hold for 2 h and cooled down in He flow to 90 °C. Then, a series of 10% $NH_3$/He or 5% $CO_2$/He pulses were introduced at 90 °C. Subsequently, the reversibly adsorbed $NH_3$ or $CO_2$

was evacuated by flowing He for 60 min. Finally, the temperature was ramped to 950 °C at a heating rate of 5 °C/min, and the signals $m/z = 17$ ($NH_3$) and 44 ($CO_2$) were monitorized (MS Pffeifer Vacuum OmniStar). The total amount of acid and basic sites was calculated from the integration of pulse areas, whereas the strength was evaluated from the corresponding TPD curve. The model reaction of skeletal isomerization of 33DM1B (3,3-dimethyl-1-butene) was used to characterize the Brønsted acid sites. The catalyst (ca. 100 mg) was in-situ reduced, and cooled down to the reaction temperature (300 °C) under inert gas-flow. The 33DM1B partial pressure and flow rate were set at 20 kPa and 15.2 mmol/h, respectively. The obtained products were online analysed by GC (column RTx-1, Restek) coupled to a flame ionization detector. The percentage of leached metal was measured by means of ICP-MS analysis of the resulting liquid aliquot.

### 2.3. Catalytic tests

The APR activity tests were carried out in a fixed-bed up-flow reactor (Microactivity Effi, PID Eng&Tech). The catalyst (particle size between 40 and 160 μm) was placed on a stainless steel frit, covered with a quartz wool plug, and in-situ reduced under 10% $H_2$/He flow at 600 °C for 2 h (heating rate 5 °C/min) at atmospheric pressure. The reactor pressure was regulated by He flow. When the desired pressure was reached, the He flow was switched to bypass and the liquid feedstream pumped into the reactor (Eldex optos 5985-1LMP pump) while the temperature was raised at 5 °C/min up to the reaction temperature. From the Weisz-Prater and Mears criteria it was confirmed that both external and intraparticle mass transfer effects were negligible in our experiments (Table S1, Supporting Information).

The product stream was cooled down to 5 °C in a Peltier device around gas-liquid separator. The gas stream was on-line analysed by GC (μGC Agilent, 4 parallel columns MS5A, PPQ, $Al_2O_3$-KCl). The gaseous products were quantified by external calibration. The liquid phase product stream was periodically sampled and analysed by either off-line GC-FID (Agilent 6890 N, HP-Wax bonded PEG column) or HPLC-RI (Waters 616, Hi-Plex H column). The liquid products identified were acetaldehyde (MeCHO), acetic acid (AcOH), acetone (ACTN), ethanol (EtOH), methanol (MeOH), ethylene glycol (EG), 1,2-propylene glycol (PG), hydroxyacetone (HA), propanal (EtCHO), propanoic acid (PA), 1-propanol (1-PrOH) and 2-propanol (2-PrOH). Pure reference compounds were used for quantification. The total organic carbon (TOC) was measured off-line on a Shimadzu TOC-L apparatus. The carbon balance was above 90% for all the experiments.

The catalytic performance was evaluated based on parameters summarized in Table 1.

**Table 1**
Reaction indices for catalytic performance evaluation.

| Reaction index | | Calculation | Analytical method | Eqn. |
|---|---|---|---|---|
| $X_{gly}$ | Glycerol conversion | $X_{gly}(\%) = 100 \times \frac{F_{gly}^{in} - F_{gly}^{out}}{F_{gly}^{in}}$ $F_{gly}^{in}$ and $F_{gly}^{out}$ are the molar flow of glycerol in the reactor inlet and outlet, respectively | HPLC | (1) |
| $X_{gas}$ | Conversion to gas | $X_{gas}(\%) = 100 \times \frac{F_C^{gas}}{3 \cdot F_{gly}^{in}}$ $F_C^{gas}$ is the carbon molar flow in the gas stream | TOC | (2) |
| $S_{H2}$ | Hydrogen selectivity | $S_{H2}(\%) = 100 \times \frac{2 \cdot F_{H2}^{out}}{F_H^{gas}}$ $F_{H2}^{out}$ and $F_H^{gas}$ are the molar flow of $H_2$ and H atoms in gas products, respectively | μGC | (3) |
| $SR_{H2}$ | Hydrogen selectivity ratio | $Y_{H2} = \frac{F_{H2}^{out}}{F_{gly}^{in} - F_{gly}^{out}}$ | μGC | (4) |
| $Y_{H2}$ | Hydrogen yield | $Y_{H2}(\%) = 100 \times \frac{F_{H2}^{out}}{7 \cdot F_{gly}^{in}}$ | μGC | (5) |
| $S_{alk}$ | Selectivity to alkanes | $S_{alk}(\%) = 100 \times \frac{F_{alk}^{out}}{F_C^{gas}}$ $F_{alk}^{out}$ and $F_C^{gas}$ are the carbon atoms in alkanes and carbon atoms in gas products, respectively | μGC | (6) |
| $Y_i$ | Yield of liquid product i | $Y_i(\%) = 100 \times \frac{F_i^{out}}{F_{gly}^{in}}$ $F_i^{out}$ is the molar flow of liquid product i | HPLC | (7) |

## 3. Results and discussion

### 3.1. Catalyst characterization

The main physico-chemical properties of the 0.3Pt/CoAl catalyst are given in Table 2. Both the actual platinum loading and the Co/Al atom ratio were close to the nominal values. Regarding textural characteristics, both the calcined and reduced forms of the solid showed mesoporous nature (Fig. S1, Supporting Information) with isotherms of type IV and H1 hysteresis, both having unimodal pore size distribution. The textural properties of the catalyst barely varied upon reduction (i.e. $S_{BET}$: 10.3% decrease; $d_{pore}$: 13.5% increase). The former feature was due to the inherently lower surface area of the metallic Co and Pt, while the latter feature suggested that Pt was mostly deposited into the smallest pores.

The $^{27}$Al NMR analysis (Fig. S2, Supporting Information) of the support Co/Al exhibited only two peaks at 6.9 and 71.8 ppm, corresponding to aluminium ions in octahedral and tetrahedral symmetry, respectively [47]. In the bare support, strongly prevails the octahedral symmetry ($Al_{octahedral}/Al_{tetrahedral}$=96/4). After Pt impregnation, a resonance peak around 33 ppm emerged, indicating the presence of penta-coordinated aluminium. This peaks represented about 8% of the total area. Concomitantly, the relative amount of octahedral aluminium decreased to 84%. These findings suggested that Pt ensembles anchored on octahedral sites.

The oxidation state and concentration of surface elements of the sample were surveyed by XPS. The Co 2p spectrum of the calcined catalyst (Fig. 1a) presented the characteristic pattern of cobalt oxide, with the Co $2p_{3/2}$ peak at 781.1 eV and a strong shake up feature at 785.1 eV. The $2p_{3/2}$-$2p_{1/2}$ line separation is 15.6 eV. These remarks virtually exclude the presence of $Co^{3+}$ ions. It is worth pointing out that during XPS analysis the beam emitted may partially reduce the cobalt oxide species. Reduction of the sample by hydrogen at 600 °C gives rise to additional Co $2p_{3/2}$ feature at 778.2 eV (Fig. 1b) that could be unambiguously assigned to metallic cobalt [48]. Detailed XPS spectra from Pt 4d and Al 2p levels for calcined and reduced samples are shown in Fig. 1c–d. The Pt $4d_{5/2}$ spectra exhibited binding energy (BE) values of 316.8 ± 0.3 eV for the calcined solid and shifted to 314.0 ± 0.3 eV for the reduced solid. According to literature, the latter denotes the presence of fully reduced metallic Pt at the catalyst surface [49]. The Al 2p peak was measured at 74.2 eV for both forms of the solid, either calcined and reduced, indicating that octahedral sites of $Al^{3+}$ cations were dominant [50].

XRD patterns of fresh and reduced solids are displayed in Fig. 2a. The calcined form of the solid showed diffraction peaks consistent with both the standard cobalt oxide (PDF 00-042-1467) and cobalt aluminate (PDF 00-044-0160) spinel structure, in agreement with the support composition. In the reduced form of the solid, additional peaks, characteristic of $Co^0$ in both *hcp* and *fcc* phases could be observed. The measured mean crystallite size of the spinel and metallic cobalt were 6.3 and 6.9 nm, respectively (Table 2). The absence of reflections attributable to platinum phases (neither in the calcined nor the reduced forms) suggested that the size domains were below conventional XRD detection limit, and could be ascribed to the low loading and high dispersion of Pt.

The $H_2$-TPR profile of the fresh calcined solid (TPRa) is shown in

**Table 2**
Physico-chemical properties of the reduced 0.3Pt/CoAl catalyst.

| Actual Pt[a] (wt%) | ActualCo/Al[a] (at./at.) | $S_{BET}$[b] ($m^2$/g) | $d_{pore}$[b] (nm) | $V_{pore}$[b] ($cm^3$/g) | $d_{spinel}$[c] (nm) | $d_{Co^o}$[c] (nm) | $S_{Pt}$[d] ($m^2_{Pt}$/g) | $S_{Co}{}^o$[d] ($m^2_{Co^o}$/g) | $D_{Pt}$ (%) | Basicity[e] ($\mu mol_{CO2}/m^2$) | Acidity[f] ($\mu mol_{NH3}/m^2$) | Activity in 33DMB1[g] ($\mu mol/m^2h$) | $H_2$ uptake ($mmol_{H2}/g_{cat}$) |
|---|---|---|---|---|---|---|---|---|---|---|---|---|---|
| 0.29 | 0.634 | 131 (146) | 14.8 (12.7) | 0.52 (0.56) | 6.3 | 6.9 | 0.44 | 2.01 | 58 | 1.16 | 0.56 | 85 | 7.285 (5.088)* |

Values in parenthesis correspond to calcined form of the solid.
[a] ICP-AES; [b] Nitrogen isotherms; [c] XRD; [d] $H_2$ chemisorption; [e] $CO_2$-TPD; [f] $NH_3$-TPD; [g] at 300 °C. * uptake up to 600 °C in $H_2$-TPR.

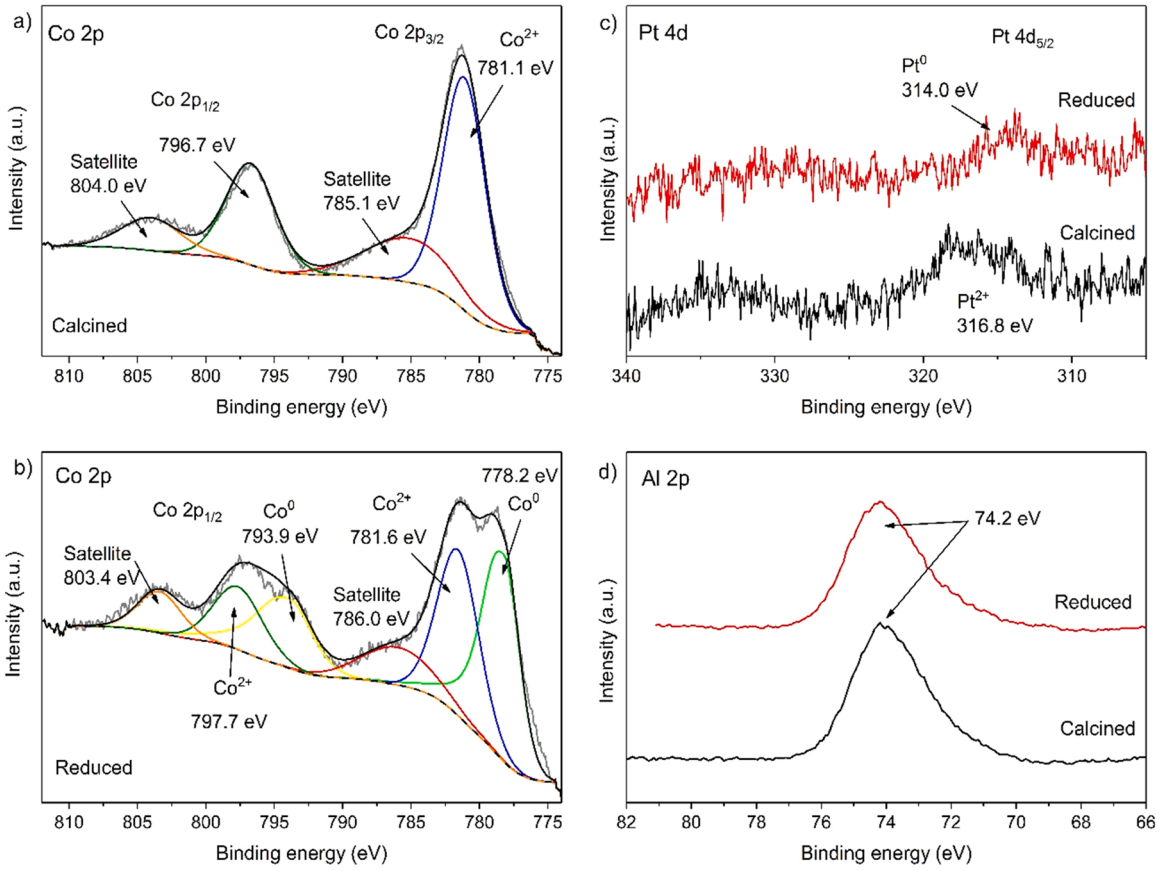


**Fig. 1.** Detailed XPS spectra of 0.3Pt/CoAl solid: Co 2p region for (a) calcined and (b) reduced solids; (c) Pt 4d region; (d) Al 2p region.

Fig. 2b, and exhibits four reduction peaks. The peak assignation was done according to [45]. The low temperature peak (at 192 °C) was ascribed to the concomitant reduction of $PtO_X$ species and free surface $Co^{3+}$ to $Co^{2+}$ species promoted by hydrogen spillover over $Pt^0$. The peak at 331 °C was ascribed to the reduction of $Co^{3+}$ species in close interaction with the support. The intense reduction peak centered at 563 °C was assigned to $Co^{2+}$ reduction to $Co^0$. Finally, the peak at 763 °C was assigned to the reduction of cobalt ions in the cobalt aluminate ($CoAl_2O_4$) phase. In order to further investigate the temperature required for full reduction of both Pt ensembles and $Co^{3+}$ species not in the aluminate spinel phase, two additional TPR experiments were done consecutively. First, TPRb, where the calcined solid was reduced up to 600 °C and hold for 1 h; subsequently, after cooling down to room temperature, sample was again reduced up to 950 °C (TPRc). The TPRb reduction profile from room temperature to 600 °C was identical to TPRa, and represented around 70% of its hydrogen uptake. The TPRc profile showed a single, broad reduction peak at 780 °C, ascribed to the reduction of the cobalt aluminate spinel. No peaks at below 625 °C were detected. Therefore, it was confirmed that both platinum species and the cobalt as segregated $Co_3O_4$ were completely reduced at 600 °C. Based on the $H_2$-TPR results, the catalyst was reduced at 600 °C for 2 h prior to the catalytic runs.

$H_2$ pulse chemisorption (Fig. S3, Supporting Information) was carried out to titrate the metallic surfaces. As expected, the catalyst reduced at 600 °C for 1 h showed about 5 times more metallic Co surface than metallic Pt surface (2.01 $m^2$/g vs 0.44 $m^2$/g). These values indicated that only 1.84% of the total surface was due to metals. For platinum, the calculated dispersion was 58% with an average diameter of 2.4 nm, in agreement with the absence of XRD peaks.

Ammonia and carbon dioxide TPD experiments revealed the amphoteric character of our spinel based catalyst (Table 2). Its surface was predominantly basic, as basic sites density was two-fold larger than acid sites density. In addition, the basic sites were primarily weak (88% contribution) while the acid sites were medium strength sites (86% contribution) (Fig. S4, Supporting Information). The very low activity in the 33DMB1 isomerization (Table 2) in comparison with other Lewis solids [51] indicated they are predominantly of Lewis-type.

### 3.2. Catalytic activity

#### 3.2.1. Reforming pathways

Based on the obtained liquid and gaseous products, Reynoso et al.

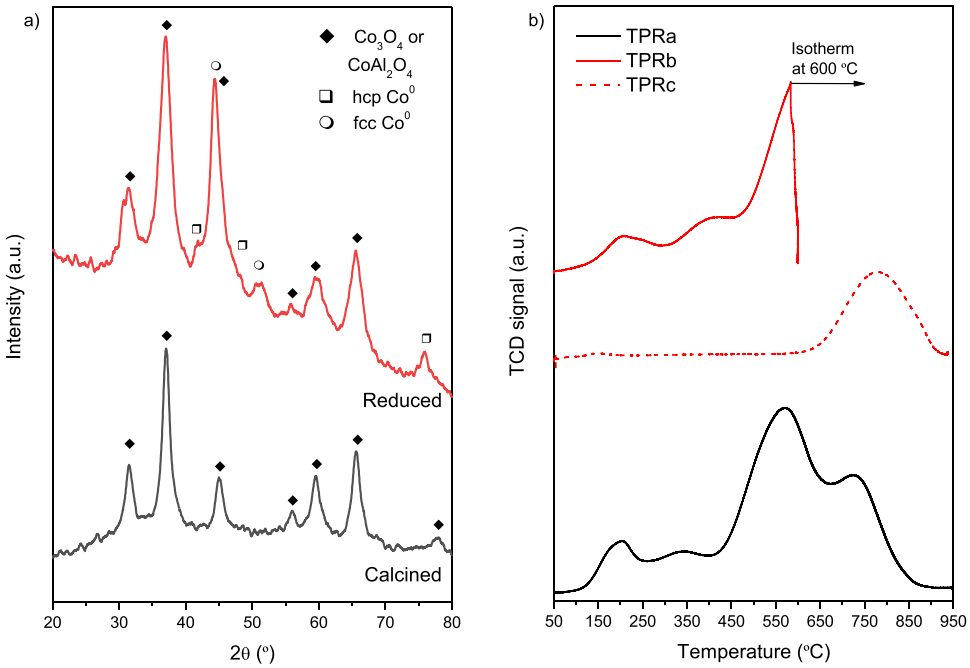


**Fig. 2.** (a) XRD of calcined and reduced 0.3PtCoAl catalyst; (b) $H_2$-TPR profile of 0.3PtCoAl: TPRa (calcined up to 950 °C), TPRb (calcined up to 600 °C), TPRc (pre-reduced up to 950 °C).

[45] suggested a plausible reaction pathway for the glycerol APR on cobalt aluminate derived catalysts. Reaction pathway consisted on two main routes, which needed both acid and metallic sites (Scheme 1). In outline, dehydrogenation to glyceraldehyde, preferably on metal sites, which undergoes decarbonylation to produce ethylene glycol, methanol and finally hydrogen. On the other hand, dehydration route, mainly on acid sites, first produces hydroxyacetone and, by subsequent dehydration/hydrogenation, yields $C_3$ liquid products. Further transformation of the liquid products due to C–O bond cleavage leads to the formation of alkanes, which decreases the evolution of hydrogen. In addition, CO can be converted by WGS, increasing $H_2$ yield, or can be hydrogenated (together with $CO_2$) to produce methane and alkanes by Fischer-Tropsch reaction, constituting a hydrogen selectivity challenge.

### 3.2.2. *Influence of the glycerol concentration in the feed*

The influence of feedstock concentration on the catalytic reaction

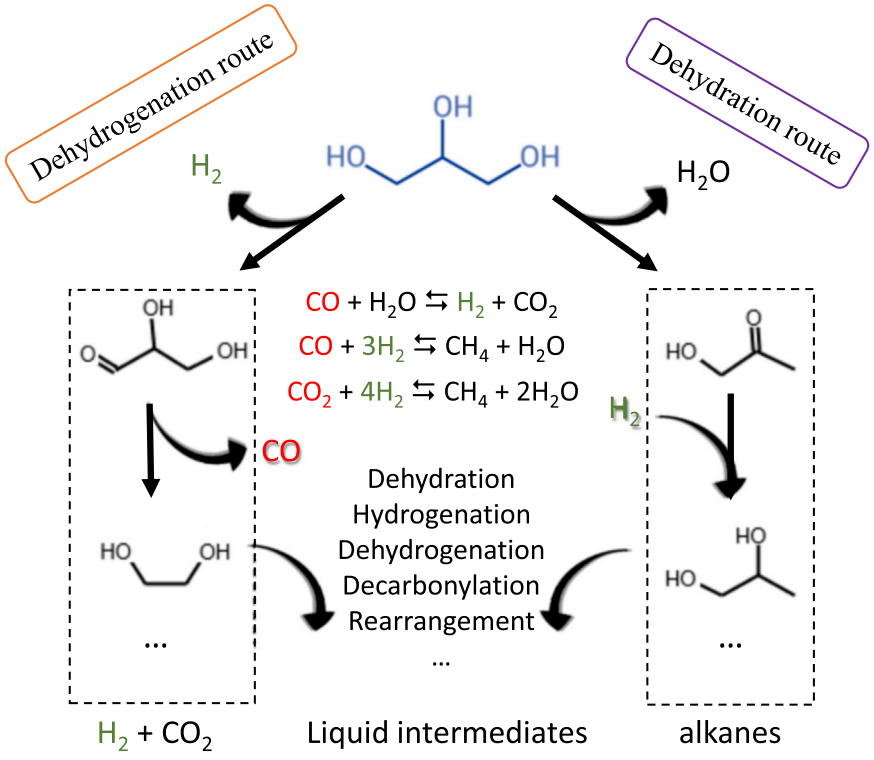


**Scheme 1.** Reaction pathways of aqueous-phase reforming of glycerol [45].

was explored at 260 °C and 50 bar, at WHSV of 6.8 $h^{-1}$ (flowrate: 0.1 mL/min, catalyst mass: 0.9 g) and varying the glycerol concentration (5, 10 and 20 wt%). Fig. 3 shows the effect of glycerol concentration in the feedstock on APR global results after 3 h TOS. The global glycerol conversion was very high (>99%) for all the glycerol concentrations, pointing to very active catalyst for glycerol reforming. Others also reported about the promotional effect of Pt-Co catalysts in the APR reactions and attributed to the PtCo alloying [30,52].

Larger differences were obtained in the carbon conversion to gas, which slightly decreased as the concentration of glycerol fed increased (e.g. 41% for lower concentration and 33% for the most concentrate feedstream). This decrease was more pronounced by increasing the glycerol content from 5% to 10%, since by increasing up to 20% the decrease was practically negligible (1.2%). This trend indicated that increasing glycerol concentration, increased the carbon content in the liquid products. Similar results were reported by others [41,53]. For more diluted feedstocks, the availability of the active sites (either metallic and acid/base) increases, thus reactions involved in the APR proceed more extensively to obtain more volatile (gas phase) compounds. Consequently, it can be deduced that feedstocks with low glycerol concentration were more advantageous for gas production (deeper degree of reforming), while more concentrated ones would be preferred for liquid production (i.e. for hydrogenolysis of glycerol by in-situ produced $H_2$) [54,55]. It could also be observed that for the WHSV values used in this study, at glycerol concentrations of 10 wt% or above, there were not enough available active sites to further decompose intermediate molecules, thus reaching almost constant $X_{gas}$. This behavior implies that reaction order with respect to glycerol concentration decreased with glycerol concentration.

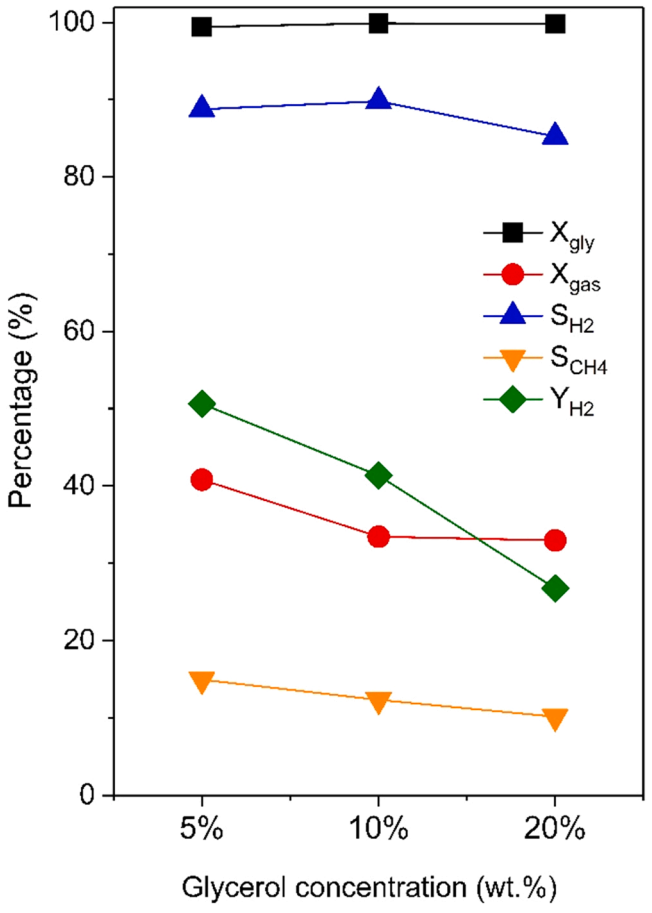


**Fig. 3.** Effect of glycerol concentration in the feedstock on glycerol APR. Operating conditions: P = 50 bar; T = 260 °C, WHSV= 6.8 $h^{-1}$, TOS= 3 h.

The most important effect of glycerol concentration was on the hydrogen yield, which showed a significant drop from 50.6% to 26.7% when glycerol concentration increased from 5% to 20%. This tendency is in line with the results reported by others [38,41] and was consistent with the above idea, that is, the surface coverage increased with glycerol concentration (i.e. less free sites being available). Moreover, the increase of liquid products yield with glycerol concentration was at the expense of hydrogen consumption, since the yield of products of hydrogenation increased (e.g. 1,2-propylene glycol).

Both selectivity to hydrogen and to alkanes showed slight decreasing trend with glycerol concentration, which was also reflected in the almost constant $H_2/CH_4$ ratio (Table 3). High values of hydrogen selectivity (above 85%) were obtained for the three feedstream compositions. Selectivity to alkanes, above 10%, was considerably high in comparison to values reported in the literature for Pt supported on alumina (around 8%) [38], and could be due to cobalt, which is active for $CO/CO_2$ hydrogenation reactions [56].

Concerning the gas product distribution (Table 3), an increase in glycerol concentration affected both $CO_2$ and $H_2$ concentration in the opposite way, increasing the former and decreasing the latter. For example, passing from 5% to 20% glycerol concentration, $H_2$ concentration decreased by 11% while $CO_2$ concentration increased by 33%. A decreasing trend for $H_2$ was reported by others [41], and was attributed to the slight increase in the yield of liquid products, being most of them formed though hydrogen consuming reactions. CO content increased with the glycerol concentration, especially at the highest glycerol concentration, due to the lower availability of free metallic centers for WGS. At the reactor outlet, $H_2/CO_2$ ratio decreased with glycerol concentration, from 3.7 to 2.5. In all cases, this ratio was above the theoretical (7/3). These results agreed with the decreasing trend of $S_{CH4}$. The lowest hydrogen concentration in the gas product was 67%, when feeding 20 wt% glycerol/water mixture. $CH_4$ content decreased slightly with the increase of glycerol content. Indeed, $H_2/CH_4$ ratio was not almost varied with glycerol concentration, which agree with the almost constant $S_{H2}$.

The $H_2$ production rate ($F_{H2}$) did not increase in proportion to the increase in glycerol concentration (see Table 3). For instance, when glycerol concentration varied from 5% to 20%, two-fold increase on $F_{H2}$ was obtained (218 vs 460 μmol/($g_{cat}$·min)) when, by stoichiometry, a 4-fold increase would be expected. Opposite trend was shown by the molar flow of hydrogen per mole of converted glycerol (i.e. hydrogen selectivity ratio $SR_{H2}$, which was limited to 7) which decreased from 3.95 to 1.44 passing from 5% to 20% glycerol feed. These features suggested that $H_2$ lost in hydrogenation/hydrogenolysis reactions increased in higher proportion by increasing the glycerol concentration.

Higher concentration of liquid products (Table 4) was obtained by increasing the glycerol content in the feed stream, in agreement with the decreasing trend of $X_{gas}$. An increase in glycerol concentration produced an increment in both hydroxyacetone (HA, primary product from glycerol dehydration) and 1,2-propylene glycol (PG, product from hydroxyacetone hydrogenation) yields. As previously reported for cobalt aluminates catalysts [57], hydrogenation reaction seems to occur more

**Table 3**
Overall results of the gas phase in the glycerol APR. Influence of the glycerol content in the feed.

| Gaseous product (vol%) | Glycerol concentration (wt%) | | |
|---|---|---|---|
| | 5 | 10 | 20 |
| $H_2$ | 75.1 | 70.8 | 67.1 |
| $CO_2$ | 20.5 | 24.5 | 27.3 |
| $CH_4$ | 3.7 | 3.6 | 3.4 |
| CO | 0.06 | 0.07 | 0.69 |
| $C_{2+}$ | 0.62 | 1.02 | 1.54 |
| $H_2/CO_2$ | 3.7 | 2.9 | 2.5 |
| $H_2/CH_4$ | 20.2 | 19.6 | 19.9 |
| $F_{H2}$, $\mu mol_{H2}/(g_{cat}\cdot min)$ | 218 | 355 | 460 |
| $SR_{H2}$ | 3.95 | 3.62 | 1.44 |

**Table 4**
Liquid products distribution varying the glycerol concentration in the feed.

| Liquid products yield, % | | Glycerol wt% | | |
|---|---|---|---|---|
| | | 5 | 10 | 20 |
| Products from dehydration route | hydroxyacetone | 4.0 | 9.1 | 9.1 |
| | 1,2-propylene glycol | 4.3 | 10.8 | 14.7 |
| | acetone | 3.5 | 4.9 | 3.8 |
| | 1-propanol | 2.0 | 3.4 | 2.1 |
| | 2-propanol | 0.23 | 0.46 | 0.18 |
| | propanoic acid | 29.0 | 26.1 | 13.3 |
| | propanal | 0.21 | 0.31 | 0.53 |
| Products from dehydrogenation route | methanol | 0.30 | 0.46 | 0.42 |
| | ethanol | 4.6 | 9.2 | 6.3 |
| | acetic acid | 4.4 | 3.6 | 1.6 |
| | acetaldehyde | 0.57 | 1.24 | 0.58 |

rapidly than dehydration. PG dehydration on acid sites can lead to the formation of acetone or propanal, depending of the primary or secondary hydroxyl elimination by dehydration [58]. Further hydrogenation of both intermediates produce 2-propanol and 1-propanol, respectively. This same route can also form propanoic acid, the main liquid product. Other authors also reported this product in the liquid stream of glycerol APR [39,59]. Among the liquid products, those whose yield was most affected corresponded to propanoic acid, which decreased at expense of the increase of hydroxyacetone and 1,2-propylene glycol, production of the later consuming hydrogen. The ratio of products from dehydrogenation route to products from dehydration route (Fig. 4) presented a maximum at 10 wt% glycerol. Therefore, it could be concluded that this glycerol concentration provides a balance between this two reaction routes. However, the yield of dehydration-route products had a more pronounced rise with glycerol concentration than those obtained via dehydrogenation-route.

### 3.2.3. *Effect of coupled temperature/pressure*

Experiments to determine the effect of coupled temperature and pressure variables on the catalyst APR performance were performed varying temperature in the 220–260 °C range, while pressure was established to ensure a liquid-phase reaction mixture (1.8–4.2 bar above the bubble point of the feedstock). This means that isolated effect of pressure was not analysed, but that of the coupled temperature and pressure. The following coupled temperature and pressure pairs were used (°C/bar): 220/25; 235/35; 245/40 and 260/50. The reaction conditions were 10 wt% glycerol concentration and WHSV= 6.8 $h^{-1}$ (0.1 mL/min of glycerol, 0.9 g of catalyst). The obtained results are shown in Fig. 5.

Conversion of glycerol reached almost 100% except for the mildest conditions ($X_{gly}$=89%), the later indicating the endothermic characteristics of the reforming reaction [60]. The lowest carbon conversion to gas (21%) was achieved at the mildest operation condition. More severe conditions enhanced carbon conversion to gas and, consequently, decreased the yield of liquid products. Despite same $X_{gly}$ trend, carbon conversion to gas exhibited a continuous increase with temperature-pressure, reaching a maximum of 43.2% at the most severe conditions (260 °C/50 bar). High temperatures promoted the reforming of glycerol and the intermediate liquids, by promotion of C-C and C-O bonds cleavage to obtain C-containing more volatile compounds [38].

The effect of couple temperature and pressure variables strongly affected hydrogen yield, which increased with temperature, in parallel with $X_{gas}$. For instance, from 220 °C/25 bar to 260 °C/50 bar an overall increment of 126% was attained by $Y_{H2}$, as due to the endothermic nature of glycerol reforming [60], which favored the glycerol decomposition. The gas products include hydrogen and C-containing compounds (see Table 5). Produced hydrogen could be further reacted giving alkanes in the gas phase and intermediate liquid compounds. Hydrogen lost in alkane formation ($S_{H2}$) was computed for each run, and the obtained trend is depicted in Fig. 5. For the mildest operation conditions, where 11% of glycerol was unreacted, selectivity to hydrogen was 88%. For the rest of conditions, where glycerol conversion was almost complete, $S_{H2}$ increased with temperature reaching a maximum of 90% at the most severe conditions. At full glycerol conversion (higher T/P conditions), APR proceeded more extensively, through the reforming of intermediate liquid products, what allowed to obtain more hydrogen. The observed decreasing yield of methane (limited by thermodynamics) indicated less hydrogen consumption, what explained the increasing hydrogen selectivity trend. Similar features for $S_{H2}$ were obtained by others [19]. Regarding alkane selectivity, it moderately increased with the operation temperature, being methane the most representative of them.

Regarding the C-atom amount of the produced alkanes, the majority corresponded to methane, which accounted for 63% at the lowest

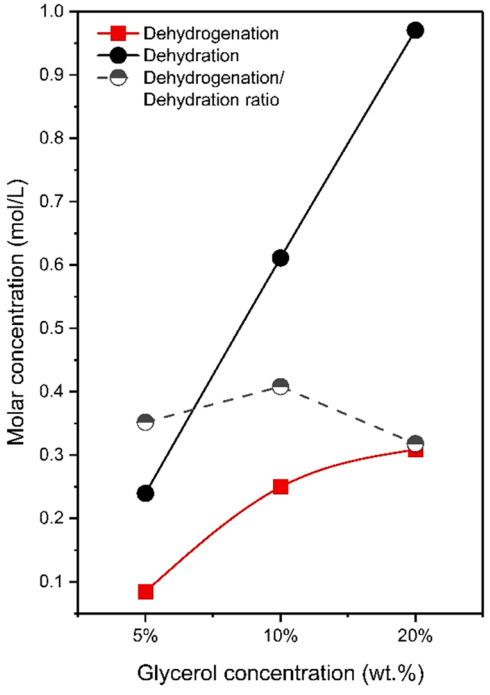


**Fig. 4.** General tendency of dehydrogenation and dehydration products in the liquid phase.

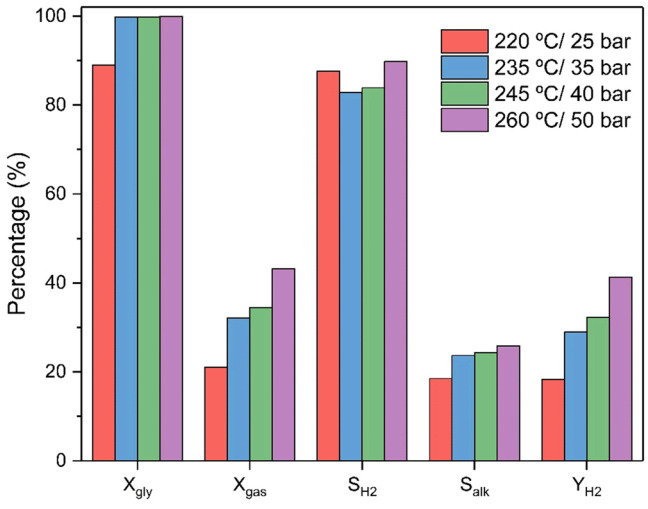


**Fig. 5.** Influence of the reaction temperature on glycerol APR performance. The following conditions were used: 10 wt% glycerol/water; WHSV = 6.8 $h^{-1}$; TOS = 3 h.

**Table 5**
Gas phase composition over 0.3Pt/CoAl at different temperature/pressure reaction.

| Gas products (vol %) | 220 °C/ 25 bar | 235 °C/ 35 bar | 245 °C/ 40 bar | 260 °C/ 50 bar |
|---|---|---|---|---|
| $H_2$ | 70.4 | 68.9 | 69.5 | 70.8 |
| $CO_2$ | 25.1 | 24.8 | 24.4 | 24.5 |
| $CH_4$ | 3.5 | 5.2 | 4.9 | 3.6 |
| CO | 0.16 | 0.10 | 0.04 | 0.07 |
| $C_2$+ | 0.87 | 0.98 | 1.17 | 1.02 |
| $H_2/CO_2$ | 2.8 | 2.8 | 2.9 | 2.9 |
| $H_2/CH_4$ | 20.3 | 13.2 | 14.2 | 16.9 |
| $F_{H2}$, $\mu mol_{H2}/(g_{cat} \cdot min)$ | 157.5 | 249.1 | 277.5 | 355.2 |
| $SR_{H2}$ | 2.49 | 2.82 | 2.99 | 3.62 |

temperature and 71% at the highest, once again suggesting that C-C scission reaction were promoted by temperature [61].

Table 5 summarizes the gas product composition. Hydrogen was, by far, the most abundant product, with around 70% mole percentage, independent of the reaction conditions. Thanks to the increasing trend in conversion to gas, $H_2$ production rate increased with temperature/pressure. $CO_2$ was the main carbon-containing product, followed by methane (3.5–5.2% range), which was the most abundant alkane. Traces of ethane, ethylene, propane, and butane were also detected (compiled as $C_2$ +). Alkanes were formed by either the subsequent reaction hydrogenation of $CO/CO_2$ and Fischer-Tropsch reactions [62]. The formation of $C_4$ + compounds suggested that Pt-Co catalysts had some activity in C-C coupling reaction, in addition to their recognized great activity in WGS reaction. The latter could be confirmed from the very low CO content in the gaseous product (< 0.2%) for all the temperatures studied.

The $H_2/CO_2$ ratio was 2.8 and 2.9 in the mildest and the most severe conditions, respectively. These values slightly exceed the theoretical value of 7/3 for glycerol APR, which indicated that glycerol was partially reformed to intermediate species that can readily undergo dehydrogenation reactions while keeping carbon atoms. The large yield of propanoic acid agreed these results.

Depending on the applied T/P conditions, around 57–79% of the carbon contained in glycerol came out in the liquid product. As the glycerol conversion reached almost 100% (except at 220 °C/25 bar, with 89%), the production of intermediate oxygenated liquids was considerable. Indeed, the spatial velocity (6.8 $h^{-1}$) was insufficient for a deep reforming of glycerol molecules. The identified liquid products (Fig. 6) comprised acids (acetic acid, propanoic acid), ketones (acetone, hydroxyacetone), aldehydes (acetaldehyde, propanal), $C_3$ alcohols (1,2-propylene glycol, 1-propanol, 2-propanol) and $C_1$-$C_2$ alcohols (ethylene glycol, ethanol, methanol). Other peaks detected by chromatography, which accounted less than 5% of all area) could not be identified. The wide variety in the liquid fraction pointed out the complexity of the glycerol APR reaction network and the strong influence of coupled temperature/pressure variable. It must be said that 1,3-propanediol was not obtained in the liquid. Formation of 1,2-propylene glycol and 1,3-propylene glycol is competitive, their selectivity depends on which intermediate, hydroxyacetone or 3-hydroxypropanal, is preferentially produced. The former intermediate is produced by Lewis acid sites [63] while the later requires Brønsted acid sites [64]. The dominant Lewis characteristics of the catalyst (Table 2) explained the absence of 1,3-propylene glycol.

Most of the liquid products contained a three-carbon chain. On the other hand, the $(C_1 + C_2)/C_3$ compounds yields ratio in the liquid stream indicated monotonous increase with the operation temperature (insert in Fig. 6) confirming that temperature promoted C-C cleavage. Most of the liquid products incremented its yield with reaction temperature, being 1,2-propylene glycol, hydroxyacetone and ethylene glycol the exceptions. The former two products resulted from the direct dehydration of glycerol (hydroxyacetone) and its subsequent hydrogenation (1,2-propylene glycol). These results indicated that an increase in reaction temperature favored the dehydrogenation pathway and explained the improvement in hydrogen yield at higher temperatures.

### 3.2.4. *Effect of contact time*

The effect of contact time was studied in terms of WHSV (higher WHSV, shorter contact time), varying the flowrate of the feedstream from 0.02 to 0.5 mL/min over 1.8 g of 0.3Pt/CoAl catalyst. The experiments were performed at 260 °C/50 bar with a 10 wt% glycerol in the feedstream. Fig. 7 shows glycerol conversion, carbon conversion to gas, hydrogen yield and selectivity to hydrogen and methane.

The effect of WHSV was very noticeable in all the parameters represented, except in $X_{gly}$, which remained close to 100% for a wide range of WHSV, only declining to 97% for the highest WHSV studied (17 $h^{-1}$).

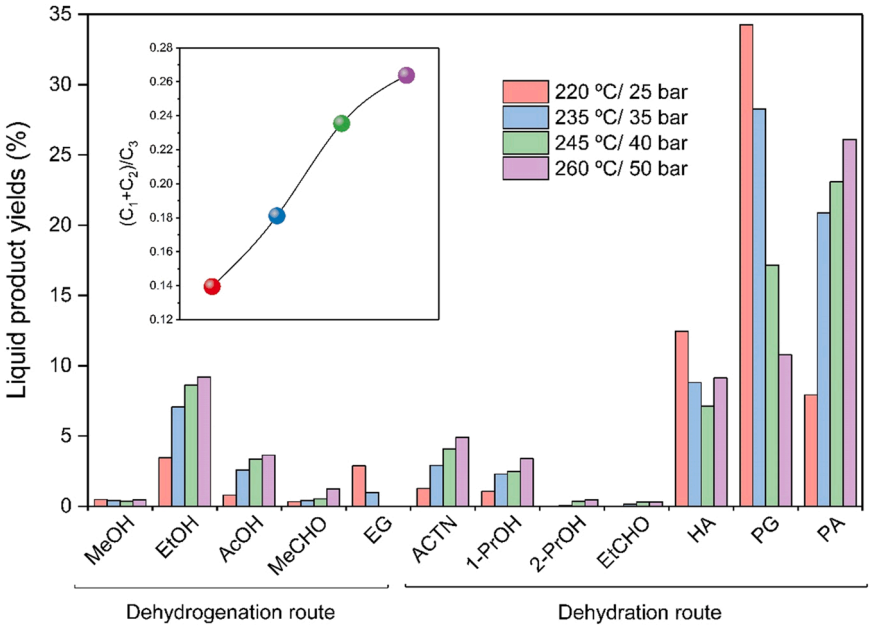


**Fig. 6.** Liquid-product yields as a function of reaction temperature of APR.

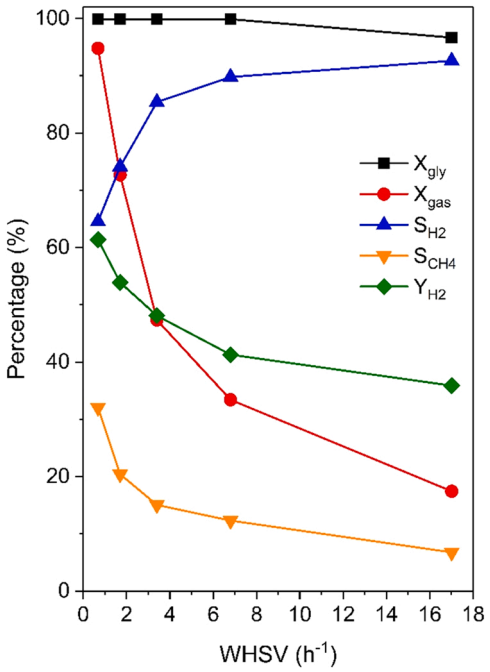


**Fig. 7.** Influence of the contact time on glycerol APR performance. Operating conditions: 50 bar, 260 °C, 10 wt% glycerol; TOS = 3 h.

These results indicated again the pronounced activity of this catalyst to glycerol decomposition, even working at very high WHSV. Nevertheless, carbon conversion to gas was highly sensitive to contact time: as WHSV increased, carbon conversion to gas decreased. Augmenting feed flowrate from 0.02 to 0.1 mL/min (WHSV = 0.68 and 3.4 $h^{-1}$, respectively) resulted in a 50% drop in the carbon conversion to gas. Further increase in WHSV resulted in a less severe decay in $X_{gas}$. Operation at high WHSV values (i.e. short contact time) hindered consecutive reforming reactions of the intermediate liquid products, thus resulting in less gaseous compounds. Similar trend was reported in the literature [19,41,59]. Interestingly, selectivity to hydrogen increased with WHSV, i.e., the shorter the contact time, less hydrogen was lost in gas phase products. Similar trend was reported by others [30] and was ascribed to a lowered rate of alkanes production. Though the space velocity employed was calculated on the liquid flowrate basis, the gases ($H_2$, CO, $CO_2$) flowed with the liquid stream. Therefore, the $S_{H2}$ trend suggested that $CO/CO_2$ hydrogenation (producing hydrogen loss in the gas phase) were lessened by the short contact times [65]. Analogous to $X_{gas}$, a decrease in hydrogen yield and selectivity to methane could be observed with WHSV, with a concomitant increase on CO and $CO_2$. This was consistent with the increase on hydrogen selectivity. At lower WHSV, the contact time between the intermediate liquids, gases and catalyst was higher, thus enhancing the hydrogen consumption reactions (such as hydrogenation $CO/CO_2$ and hydrogenolysis of the substrate and liquid intermediates) which decreased the hydrogen yield. Regarding $SR_{H2}$, it decreased with WHSV, passing from 3.89 to 1.27 $mol_{H2}/mol_{Glyc\text{-}converted}$ when WHSV increased from 0.68 to 17 $h^{-1}$.

The $CO/H_2$ molar ratio in the gas stream increased with WHSV (Fig. 8), i.e. long contact time favored WGS reaction, thus this reaction occurs to a lesser extent at high WHSV. The $H_2/CO_2$ ratio indicates the competition between C–C and C–O scission [66]. This value was slightly higher than the theoretical one (7/3) and practically remained above 2.7 regardless of the WHSV used, which indicated that 0.3Pt/CoAl catalyst had a high capacity for C-C bonds breakage prior to C-O bond breakage.

The liquid products yields at different WHSV are provided in Fig. 9. As seen before, low WHSV presented an exceptionally high carbon conversion to gas, and therefore, the yield to liquid products was insignificant. Largely, the yield of the liquid products increased with

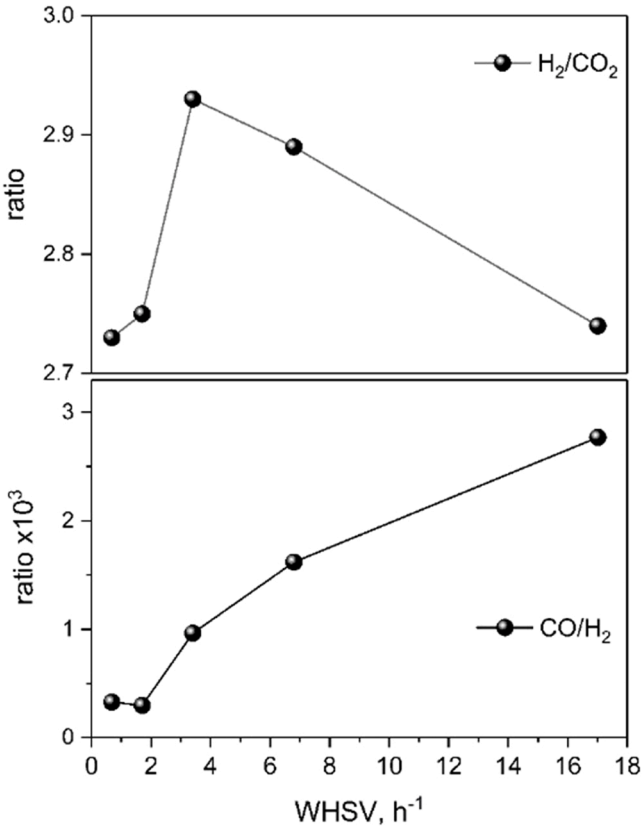


**Fig. 8.** Variation of $H_2/CO_2$ and $CO/H_2$ ratios with WHSV.

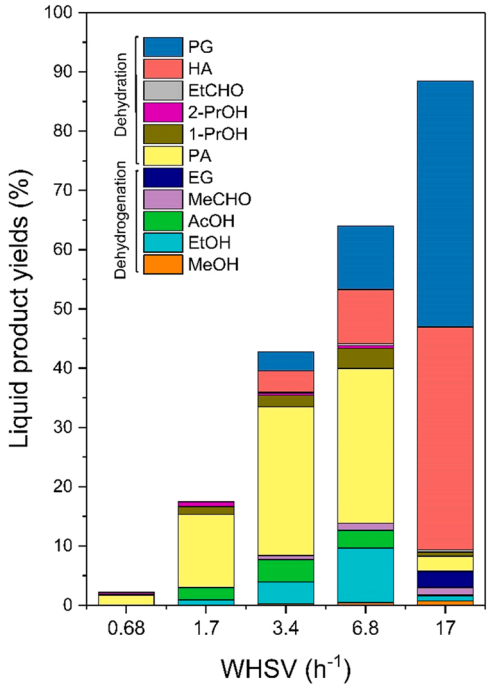


**Fig. 9.** Liquid phase composition obtained for glycerol APR at various contact time.

WHSV, in accordance with $X_{gas}$ decrease. At higher WHSV, a wide variety of liquid products could be distinguished. Among the products obtained, a noticeably high yield of hydroxyacetone and 1,2-propylene glycol could be noted at the shortest contact time (yields of 37.6% and

41.5%, respectively). The yields of both compounds increased in similar way with WHSV, which suggests that at such short contact times, dehydration and hydrogenation reactions predominate at the same rate to the detriment of C-C cleavage. This lower activity for C-C bond scission caused a drop in the yield of $C_2$ products from 13.4% at 6.8 $h^{-1}$ to 5% at 17 $h^{-1}$. Yields of propanoic acid, ethanol, acetone and both 1-propanol and 2-propanol reached their maxima at 3.4 and 6.8 $h^{-1}$, respectively, then decreasing dramatically as WHSV achieved 17.0 $h^{-1}$. It is evident that at short contact times less fragmentation of the initial molecule takes place. Contrariwise, for the longest contact time (0.68 $h^{-1}$), it is only possible to detect compounds resulting from several reaction stages such as propanols and acetone.

### 3.2.5. Characterization of spent catalysts

After each reaction at different T/P conditions, the spent catalysts were analysed by analysed by $N_2$ adsorption-desorption isotherms, XRD, ICP-MS and TPH analyses. The nitrogen isotherms and BHJ pore size distribution are shown in Fig. S5, Supporting Information. They still showed type IV isotherms with H1 hysteresis. The most notable differences with respect to the reduced form is that hysteresis loops were narrower in the spent catalysts, though they retained mesoporosity. In the spent catalysts, new generated small pores of around 4 nm contributed to the total pore volume, suggesting the presence of new phases not observed in the fresh reduced form (e.g. gibbsite). As can be seen in Table 6, the specific surface area of the spent catalyst increased when the reaction was performed at the mildest condition (18% increase at 220 °C/25 bar) while decreased for the other conditions tested (14% decrease at the most severe conditions). At lower temperatures, a greater decrease in the average pore diameter was also observed (decreased by 36% at the mildest conditions), which had a tendency to increase with the reaction temperature without reaching the value of its reduced state. XRD diffractograms of the spent catalysts (Fig. S6, Supporting Information) showed peaks from cobalt spinel (either cobalt oxide and cobalt aluminate) and metallic Co, which remained in the spent catalysts. The later suggested that bulk cobalt remained in metallic form. As in the fresh catalysts, no peaks from Pt were visible, indicating that Pt remained highly dispersed. New, sharp peak emerged for the spent catalysts at about 18º (2θ), which could be ascribed to the gibbsite phase (PDF 033-0018). The intensity of the gibbsite peak decreased with the operation temperature/pressure. The same trend observed in the textural properties indicated that gibbsite is surely related to this textural trend.

Metal leaching in the liquid product was also investigated by ICP-MS. The results showed that the reaction conditions influenced cobalt leaching. Although the overall results confirmed low metal leaching, cobalt was found to be more leachable at low reaction temperatures (cobalt leaching was 2.30% after reaction at 220 °C vs 0.74% at 235 °C). These apparently inconsistent results agreed with results obtained with catalyst 0.625CoAl after 30 h TOS at 235 °C and 260 °C [57]. A comprehensible explanation could be found in the re-deposition of hydroxylated alumina. At higher temperatures, pH of the reaction medium increased, thus greater leaching was expected. However, in hot water the solubility of the inorganic oxide materials is low, which facilitates the re-deposition of leached alumina, decorating the cobalt and therefore protecting it from leaching [67]. This was in agreement with the gibbsite phase detected by XRD. As for the other metals, both platinum and aluminium had a low percentage of leaching (below $4{\cdot}10^{-3}$% and 0.02%, respectively), understanding that the platinum conferred the stability of the catalyst during reaction. The production of stable catalysts against leaching is a challenge in biomass transformation processes. The most researched strategies to stabilize the supported metal nanoparticles focus on overcoat using techniques such as Atomic Layer Deposition (ALD) [68] or the embedment into support structure via strong metal–support interaction (SMSI) [69–71].

The quantification of the carbonaceous deposits was measured by TPH (Temperature-Programmed Hydrogenation). The results obtained by TPH did not show any relation to the reaction condition. The samples with the highest amount of carbonaceous deposits correspond to those for the reactions at 235 and 245 °C. Surprisingly, the catalysts after the reaction at 260 °C had a content of carbonaceous material very similar to that used in the reaction at 220 °C (about 3 times less than at the other conditions). It is worth highlighting the much lower (three to four orders of magnitude) coke deposits in glycerol APR as compared to glycerol steam reforming [72,73]. This was due to the ability of hot compressed water to dissolve carbonaceous deposits [67].

**Table 6**
Physicochemical properties of spent catalyst.

| Operation T/P conditions | $S_{BET}$ ($m^2$/g) | $V_{pore}$ ($cm^3$/g) | $d_{pore}$ (nm) | Leaching metal (wt%) | | | Carbon deposits ($\mu mol_C/g_{cat}$) |
|---|---|---|---|---|---|---|---|
| | | | | Pt | Co | Al | |
| Fresh reduced | 131 | 0.52 | 14.8 | n.a. | n.a. | n.a. | n.a. |
| 220 °C/ 25 bar | 155 | 0.42 | 9.5 | – | 2.30 | 0.02 | 1.62 |
| 235 °C/ 35 bar | 119 | 0.40 | 10.7 | $1.77{\cdot}10^{-3}$ | 0.74 | 0.01 | 4.39 |
| 245 °C/ 40 bar | 116 | 0.38 | 11.1 | $1.77{\cdot}10^{-3}$ | 0.67 | 0.01 | 5.25 |
| 260 °C/ 50 bar | 113 | 0.40 | 12.1 | $4.13{\cdot}10^{-3}$ | 0.37 | 0.01 | 1.75 |

## 4. Conclusions

0.3Pt/CoAl catalyst, synthesized by impregnation of Pt over cobalt aluminate (nominal Co/Al = 0.625) support, was characterized and tested for glycerol aqueous-phase reforming under various reaction conditions. Specifically, the glycerol concentration in the feedstream, the coupled temperature/pressure variable and the space velocity (in terms of WHSV) process variables were studied. At the conditions studied (260 °C/50 bar), the glycerol conversion did not show significant variation when glycerol concentration was increased from 5 to 20 wt% nor when the space velocity was increased from 0.68 to 6.8 $h^{-1}$. Only at 220 °C/25 bar (WHSV = 6.8 $h^{-1}$, 10 wt% glycerol/water) did the glycerol conversion drop below 90%. The highest carbon conversion to gas was achieved at a lower glycerol concentration, at highest temperature/pressure, and at lengthy contact time. As expected, the conditions where the highest conversion to gas was achieved were the ideal ones to obtain higher hydrogen yield.

Increasing the glycerol concentration in the feedstream from 5% to 20% (260 °C/50 bar, 10 wt% glycerol/water, WHSV = 6.8 $h^{-1}$) also showed an increase in the yield of the liquid products formed through the dehydration/hydrogenation of glycerol such as hydroxyacetone and propylene glycol. Conversely, by increasing temperature/pressure from 220 °C/25 bar to 260 °C/50 bar (10 wt% glycerol/water, WHSV = 6.8 $h^{-1}$) 1,2-propylene glycol yield decreased while ethanol yield increased. As well, higher hydrogen yield was achieved at a higher reaction temperature. On the topic of post-reaction characterization, temperature/pressure conditions undoubtedly affected cobalt leaching. However, further investigation is needed to clearly establish leaching mechanism, which will help to overcome this challenge.

Increasing the feed flowrate, and consequently the WHSV, did not change the composition of the outflow gases. Nonetheless, due to the shorter contact time, the production of liquids increased, especially the liquids obtained by the direct reaction of glycerol (hydroxyacetone and 1,2-propylene glycol).

## CRediT authorship contribution statement

**A. J. Reynoso:** Investigation and Writing – original draft. **J.L. Ayastuy:** Funding acquisition, Conceptualization, Writing – review &

editing. **U. Iriarte-Velasco:** Formal analysis, Writing – review & editing. **M.A. Gutiérrez-Ortiz:** Resources, Funding acquisition and Supervision.

## Declaration of Competing Interest

The authors declare that they have no known competing financial interests or personal relationships that could have appeared to influence the work reported in this paper.

## Acknowledgements

This research was supported by grant PID2019-106692EB-I00 funded by MCIN/ AEI/10.13039/501100011033. The authors thank for technical support provided by SGIker of UPV/EHU and European funding (ERDF and ESF).

## Appendix A. Supporting information

Supplementary data associated with this article can be found in the online version at doi:10.1016/j.jece.2022.107402.

## References

[1] S. Solomon, G. Plattner, R. Knutti, P. Friedlingstein, Irreversible climate change due to carbon dioxide emissions, Proc. Natl. Acad. Sci. USA, 106 (2009) 1704–1709.
[2] M.K. Cohce, I. Dincer, M.A. Rosen, Energy and exergy analyses of a biomass-based hydrogen production system, Bioresour. Technol. 102 (2011) 8466–8474.
[3] T. Lepage, M. Kammoun, Q. Schmetz, A. Richel, Biomass-to-hydrogen: a review of main routes production, processes evaluation and techno-economical assessment, Biomass Bioenergy 144 (2021), 105920.
[4] J.O. Abe, A.P.I. Popoola, E. Ajenifuja, O.M. Popoola, Hydrogen energy, economy and storage: Review and recommendation, Int. J. Hydrog. Energy 44 (2019) 15072–15086.
[5] H.T. Hwang, A. Varma, Hydrogen storage for fuel cell vehicles, Curr. Opin. Chem. Eng. 5 (2014) 42–48.
[6] K. Mazloomi, C. Gomes, Hydrogen as an energy carrier: prospects and challenges, Renew. Sustain. Energy Rev. 16 (2012) 3024–3033.
[7] T. Lepage, M. Kammoun, Q. Schmetz, A. Richel, Biomass-to-hydrogen: a review of main routes production, processes evaluation and techno-economical assessment, Biomass Bioenergy 144 (2021), 105920.
[8] Y.A. Situmorang, Z. Zhao, P. An, T. Yu, J. Rizkiana, A. Abudula, G. Guan, A novel system of biomass-based hydrogen production by combining steam bio-oil reforming and chemical looping process, Appl. Energy 268 (2020), 115122.
[9] H. Li, Y. Wang, N. Zhou, L. Dai, W. Deng, C. Liu, Y. Cheng, Y. Liu, K. Cobb, P. Chen, R. Ruan, Applications of calcium oxide–based catalysts in biomass pyrolysis/ gasification – a review, J. Clean. Prod. 291 (2021), 125826.
[10] C.C. Chong, Y.W. Cheng, K.H. Ng, D.V.N. Vo, M.K. Lam, J.W. Lim, Bio-hydrogen production from steam reforming of liquid biomass wastes and biomass-derived oxygenates: a review, Fuel 311 (2022), 122623.
[11] M. Alvear, A. Aho, I.L. Simakova, H. Grénman, T. Salmi, D.Y. Murzin, Aqueous phase reforming of alcohols over a bimetallic Pt-Pd catalyst in the presence of formic acid, Chem. Eng. J. 398 (2020), 125541.
[12] G. Zoppi, G. Pipitone, R. Pirone, S. Bensaid, Aqueous phase reforming process for the valorization of wastewater streams: application to different industrial scenarios, Catal. Today, in press. ⟨https://doi.org/10.1016/j.cattod.2021.06.002⟩.
[13] R.D. Cortright, R.R. Davda, J.A. Dumesic, Hydrogen from catalytic reforming of biomass-derived hydrocarbons in liquid water, Nature 418 (2002) 964–967.
[14] R.L. Manfro, A.F. Da Costa, N.F.P. Ribeiro, M.M.V.M. Souza, Hydrogen production by aqueous-phase reforming of glycerol over nickel catalysts supported on $CeO_2$, Fuel Process. Technol. 92 (2011) 330–335.
[15] J.J. Bozell, G.R. Petersen, Technology development for the production of biobased products from biorefinery carbohydrates—the US Department of Energy's "Top 10" revisited, Green Chem. 12 (2010) 539–554.
[16] Z. Gholami, A.Z. Abdullah, K. Lee, Dealing with the surplus of glycerol production from biodiesel industry through catalytic upgrading to polyglycerols and other value-added products, Renew. Sustain. Energy Rev. 39 (2014) 327–341.
[17] I. Coronado, M. Stekrova, M. Reinikainen, P. Simell, L. Lefferts, J. Lehtonen, A review of catalytic aqueous-phase reforming of oxygenated hydrocarbons derived from biorefinery water fractions, Int. J. Hydrog. Energ. 41 (2016) 11003–11032.
[18] J. Callison, N.D. Subramanian, S.M. Rogers, A. Chutia, D. Gianolio, C.R.A. Catlow, P.P. Wells, N. Dimitratos, Directed aqueous-phase reforming of glycerol through tailored platinum nanoparticles, Appl. Catal. B Environ. 238 (2018) 618–628.
[19] H. Kim, H.J. Park, T. Kim, K. Jeong, H. Chae, S. Jeong, H.J. Chae, S.Y. Jeong, C. H. Lee, C.U. Kim, The effect of support and reaction conditions on aqueous phase reforming of polyol over supported Pt–Re bimetallic catalysts, Catal. Today 185 (2012) 73–80.
[20] A.S. Oliveira, T. Cordero-Lanzac, J.A. Baeza, L. Calvo, F. Heras, J.J. Rodriguez, M. A. Gilarranz, Continuous aqueous phase reforming of a synthetic brewery wastewater with Pt/C and PtRe/C catalysts for biohydrogen production, Chemosphere 281 (2021), 130885.
[21] F. Bossola, X.I. Pereira-Hernández, C. Evangelisti, Y. Wang, V. Dal Santo, Investigation of the promoting effect of Mn on a Pt/C catalyst for the steam and aqueous phase reforming of glycerol, J. Catal. 349 (2017) 75–83.
[22] T. Numpilai, C.K. Cheng, A. Seubsai, K. Faungnawakij, J. Limtrakul, T. Witoon, Sustainable utilization of waste glycerol for 1,3-propanediol production over Pt/ $WOx/Al_2O_3$ catalysts: effects of catalyst pore sizes and optimization of synthesis conditions, Environ. Pollut. 272 (2021), 116029.
[23] A. Larimi, F. Khorasheh, Renewable hydrogen production over $Pt/Al_2O_3$ nano-catalysts: Effect of M-promoting (M=Pd, Rh, Re, Ru, Ir, Cr), Int. J. Hydrog. Energy 44 (2019) 8243–8251.
[24] H. Harju, G. Pipitone, L. Lefferts, Influence of the catalyst particle size on the aqueous phase reforming of n-butanol over $Rh/ZrO_2$, Front. Chem. 8 (2020), 17 article 17.
[25] M.I. Shahbudin, D.M. Jacob, M. Ameen, A. Aqsha, M.T. Azizan, M.H.M. Yusoff, F. Sher, Liquid value-added chemicals production from aqueous phase reforming of sorbitol and glycerol over sonosynthesized Ni-based catalyst, J. Environ. Chem. Eng. 9 (2021), 105766.
[26] A. Syuhada, M. Ameen, F. Sher, M.T. Azizan, A. Aqsha, M.H. Yusoff, M.S.H. Ruslan, Effect of calcium doping using aqueous phase reforming of glycerol over sonochemically synthesized nickel-based supported $ZrO_2$ catalyst, Catalysts 11 (2021) 977.
[27] R. Raso, L. García, J. Ruiz, M. Oliva, J. Arauzo, Aqueous phase hydrogenolysis of glycerol over Ni/Al-Fe catalysts without external hydrogen addition, Appl. Catal. B Environ. 283 (2021), 119598.
[28] I. Coronado, M. Stekrova, L. García Moreno, M. Reinikainen, P. Simell, R. Karinen, J. Lehtonen, Aqueous-phase reforming of methanol over nickel-based catalysts for hydrogen production, Biomass Bioenergy 106 (2017) 29–37.
[29] F. Bastan, M. Kazemeini, A. Larimi, H. Maleki, Production of renewable hydrogen through aqueous-phase reforming of glycerol over $Ni/Al_2O_3MgO$ nano-catalyst, Int. J. Hydrog. Energy 43 (2018) 614–621.
[30] P.J. Dietrich, M.C. Akatay, F.G. Sollberger, E.A. Stach, J.T. Miller, W.N. Delgass, F. H. Ribeiro, Effect of Co loading on the activity and selectivity of PtCo aqueous phase reforming catalysts, ACS Catal. 4 (2014) 480–491.
[31] J. Tao, L. Hou, B. Yan, G. Chen, W. Li, H. Chen, Z. Cheng, F. Lin, Hydrogen production via aqueous-phase reforming of ethylene glycol over a nickel–iron alloy catalyst: effect of cobalt addition, Energy Fuels 34 (2020) 1153–1161.
[32] S.D. Davidson, J. Sun, Y. Hong, A.M. Karim, A.K. Datye, Y. Wang, The effect of ZnO addition on Co/C catalyst for vapor and aqueous phase reforming of ethanol, Catal. Today 233 (2014) 38–45.
[33] M. El Doukkali, A. Iriondo, I. Gandarias, Enhanced catalytic upgrading of glycerol into high value-added $H_2$ and propanediols: recent developments and future perspectives, Mol. Catal. 490 (2020), 110928.
[34] L.A. Dosso, C.R. Vera, J.M. Grau, Aqueous phase reforming of polyols from glucose degradation by reaction over Pt/alumina catalysts modified by Ni or Co, Int. J. Hydrog. Energy 42 (2017) 18853–18864.
[35] C. He, J. Zheng, K. Wang, H. Lin, J. Wang, Y. Yang, Sorption enhanced aqueous phase reforming of glycerol for hydrogen production over Pt-Ni supported on multi-walled carbon nanotubes, Appl. Catal. B Environ. 162 (2015) 401–411.
[36] S. Jeon, Y.M. Park, K. Saravanan, G.Y. Han, B. Kim, J. Lee, J.W. Bae, Aqueous phase reforming of ethylene glycol over bimetallic platinum-cobalt on ceria–zirconia mixed oxide, Int. J. Hydrog. Energy 42 (2017) 9892–9902.
[37] D. Li, Y. Li, X. Liu, Y. Guo, C. Pao, J. Chen, Y. Hu, Y. Wang, $NiAl_2O_4$ spinel supported Pt catalyst: high performance and origin in aqueous-phase reforming of methanol, ACS Catal. 9 (2019) 9671–9682.
[38] N. Luo, X. Fu, F. Cao, T. Xiao, P.P. Edwards, Glycerol aqueous phase reforming for hydrogen generation over Pt catalyst - effect of catalyst composition and reaction conditions, Fuel 87 (2008) 3483–3489.
[39] J. Remón, J.R. Giménez, A. Valiente, L. García, J. Arauzo, Production of gaseous and liquid chemicals by aqueous phase reforming of crude glycerol: influence of operating conditions on the process, Energy Convers. Manag. 110 (2016) 90–112.
[40] Y. Guo, X. Liu, M.U. Azmat, W. Xu, J. Ren, Y. Wang, G. Lu, Hydrogen production by aqueous-phase reforming of glycerol over Ni-B catalysts, Int. J. Hydrog. Energy 37 (2012) 227–234.
[41] L. García, A. Valiente, M. Oliva, J. Ruiz, J. Arauzo, Influence of operating variables on the aqueous-phase reforming of glycerol over a Ni/Al coprecipitated catalyst, Int. J. Hydrog. Energy 43 (2018) 20392–20407.
[42] D. Roy, B. Subramaniam, R.V. Chaudhari, Aqueous phase hydrogenolysis of glycerol to 1,2-propanediol without external hydrogen addition, Catal. Today 156 (2010) 31–37.
[43] A. Seretis, P. Tsiakaras, Aqueous phase reforming (APR) of glycerol over platinum supported on $Al_2O_3$ catalyst, Renew. Energy 85 (2016) 1116–1126.
[44] D.Ö. Özgür, B.Z. Uysal, Hydrogen production by aqueous phase catalytic reforming of glycerine, Biomass Bioenergy 35 (2011) 822–826.
[45] A.J. Reynoso, U. Iriarte-Velasco, M.A. Gutiérrez-Ortiz, J.L. Ayastuy, Highly stable $Pt/CoAl_2O_4$ catalysts in aqueous-phase reforming of glycerol, Catal. Today 367 (2020) 278–289.
[46] G. Bergeret, P. Gallezot, Particle size and dispersion measurements, handbook of heterogeneous, Catalysis (2008) 738–765.
[47] C.V. Chandran, C.E.A. Kirschhock, S. Radhakrishnan, F. Taulelle, J.A. Martens, E. Breynaert, Alumina: discriminative analysis using 3D correlation of solid-state NMR parameters, Chem. Soc. Rev. 48 (2019) 134–156.

[48] M.C. Biesinger, B.P. Payne, A.P. Grosvenor, L.W.M. Lau, A.R. Gerson, R.S.C. Smart, Resolving surface chemical states in XPS analysis of first row transition metals, oxides and hydroxides: Cr, Mn, Fe, Co and Ni, Appl. Surf. Sci. 257 (2011) 2717–2730.
[49] N.S. Resende, C.A. Perez, J.G. Eon, M. Schmal, The effect of coating $TiO_2$ on the CO oxidation of the Pt/γ-alumina catalysts, Catal. Lett. 141 (2011) 1685–1692.
[50] A.A. Khassin, T.M. Yurieva, V.V. Kaichev, V.I. Bukhtiyarov, A.A. Budneva, E. A. Paukshtis, V.N. Parman, Metal–support interactions in cobalt-aluminum co-precipitated catalysts: XPS and CO adsorption studies, J. Mol. Catal. A Chem. 175 (2001) 189–204.
[51] S.N. Delgado, D. Yap, L. Vivier, C. Especel, Influence of the nature of the support on the catalytic properties of Pt-based catalysts for hydrogenolysis of glycerol, J. Mol. Catal. A Chem. 367 (2013) 89–98.
[52] X. Wang, N. Li, L.D. Pfefferle, G.L. Haller, Pt–Co bimetallic catalyst supported on single walled carbon nanotube: XAS and aqueous phase reforming activity studies, Catal. Today 146 (2009) 160–165.
[53] A. Kirilin, A. Tokarev, E. Murzina, L. Kustov, J. Mikkola, D. Murzin, Reaction products and transformations of intermediates in the aqueous-phase reforming of sorbitol, ChemSusChem 3 (2010) 708–718.
[54] N. Raju, V. Rekha, B. Abhishek, P.M. Kumar, C. Sumana, N. Lingaiah, Studies on continuous selective hydrogenolysis of glycerol over supported Cu–Co bimetallic catalysts, New J. Chem. 44 (2020) 3122–3128.
[55] E.S. Vasiliadou, A.A. Lemonidou, Kinetic study of liquid-phase glycerol hydrogenolysis over $Cu/SiO_2$ catalyst, Chem. Eng. J. 231 (2013) 103–112.
[56] R. Liu, D. Leshchev, E. Stavitski, M. Juneau, J.N. Agwara, M.D. Porosoff, Selective hydrogenation of $CO_2$ and CO over potassium promoted Co/ZSM-5, Appl. Catal. B Environ. 284 (2021), 119787.
[57] A.J. Reynoso, J.L. Ayastuy, U. Iriarte-Velasco, M.A. Gutiérrez-Ortiz, Cobalt aluminate spinel-derived catalysts for glycerol aqueous phase reforming, Appl. Catal. B Environ. 239 (2018) 86–101.
[58] T.D. Courtney, V. Nikolakis, G. Mpourmpakis, J.G. Chen, D.G. Vlachos, Liquid-phase dehydration of propylene glycol using solid-acid catalysts, Appl. Catal. A Gen. 449 (2012) 59–68.
[59] A. Wawrzetz, B. Peng, A. Hrabar, A. Jentys, A.A. Lemonidou, J.A. Lercher, Towards understanding the bifunctional hydrodeoxygenation and aqueous phase reforming of glycerol, J. Catal. 269 (2010) 411–420.
[60] A. Seretis, P. Tsiakaras, A thermodynamic analysis of hydrogen production via aqueous phase reforming of glycerol, Fuel Process. Technol. 134 (2015) 107–115.
[61] A. Seretis, P. Tsiakaras, Hydrogenolysis of glycerol to propylene glycol by in situ produced hydrogen from aqueous phase reforming of glycerol over $SiO_2$-$Al_2O_3$ supported nickel catalyst, Fuel Process. Technol. 142 (2016) 135–146.
[62] R.R. Davda, J.W. Shabaker, G.W. Huber, R.D. Cortright, J.A. Dumesic, A review of catalytic issues and process conditions for renewable hydrogen and alkanes by aqueous-phase reforming of oxygenated hydrocarbons over supported metal catalysts, Appl. Catal. B Environ. 56 (2005) 171–186.
[63] S. Zhu, X. Gao, Y. Zhu, Y. Li, Promoting effect of WOx on selective hydrogenolysis of glycerol to 1,3-propanediol over bifunctional $Pt–WOx/Al_2O_3$ catalysts, J. Mol. Catal. A Chem. 398 (2015) 391–398.
[64] D. Sun, Y. Yamada, S. Sato, W. Ueda, Glycerol hydrogenolysis into useful C3, Chem., Appl. Catal. B Environ. 193 (2016) 75–92.
[65] Z. He, X. Wang, S. Gao, T. Xiao, Effect of reaction variables on CO methanation process over $NiO–La_2O_3–MgO/Al_2O_3$ catalyst for coal to synthetic natural gas, Appl. Petrochem. Res. 5 (2015) 413–417.
[66] D.L. King, L. Zhang, G. Xia, A.M. Karim, D.J. Heldebrant, X. Wang, T. Peterson, Y. Wang, Aqueous phase reforming of glycerol for hydrogen production over Pt-Re supported on carbon, Appl. Catal. B Environ. 99 (2010) 206–213.
[67] D.J.M. de Vlieger, B.L. Mojet, L. Lefferts, K. Seshan, Aqueous phase reforming of ethylene glycol – role of intermediates in catalyst performance, J. Catal. 292 (2012) 239–245.
[68] G. Pipitone, G. Zoppi, R. Pirone, S. Bensaid, A critical review on catalyst design for aqueous phase reforming, Int. J. Hydrog. Energy 47 (2022) (2021) 151–180.
[69] F. Héroguel, B. Rozmysowicz, J.S. Luterbacher, Improving heterogeneous catalyst stability for liquid-phase biomass conversion and reforming, Chimia 69 (2015) 582–591.
[70] J. Lee, S.P. Burt, C.A. Carrero, A.C. Alba-Rubio, I. Ro, B.J. O'Neill, H.J. Kim, D.H. K. Jackson, T.F. Kuech, I. Hermans, J.A. Dumesic, G.W. Huber, Stabilizing cobalt catalysts for aqueous-phase reactions by strong metal-support interaction, J. Catal. 330 (2015) 19–27.
[71] J. Liu, B. Sun, J. Hu, Y. Pei, H. Li, M. Qiao, Aqueous-phase reforming of ethylene glycol to hydrogen on $Pd/Fe_3O_4$ catalyst prepared by co-precipitation: metal–support interaction and excellent intrinsic activity, J. Catal. 274 (2010) 287–295.
[72] K.N. Papageridis, G. Siakavelas, N.D. Charisiou, D.G. Avraam, L. Tzounis, K. Kousi, M.A. Goula, Comparative study of Ni, Co, Cu supported on γ-alumina catalysts for hydrogen production via the glycerol steam reforming reaction, Fuel Process. Technol. 152 (2016) 156–175.
[73] D. Aman, D. Radwan, M. Ebaid, S. Mikhail, E. van Steen, Comparing nickel and cobalt perovskites for steam reforming of glycerol, Mol. Catal. 452 (2018) 60–67.